

# Source Characterization of Nevada Test Site Explosions and Western U.S. Earthquakes using $Lg$ Waves: Implications for Regional Source Discrimination

by Ghassan I. Al-Eqabi, Keith D. Koper,\* and Michael E. Wysession

**Abstract** An investigation is made of the  $Lg$  waves from 15 nuclear tests at the Nevada Test Site (NTS) and 25 shallow western United States earthquakes to obtain a scheme for discriminating between possible source mechanisms. The data were recorded at four broadband stations, operated by Lawrence Livermore National Laboratory (LLNL), which encircle the NTS. The  $Lg$  wave spectra are modeled through a genetic algorithm search to find optimal values for (1) the seismic moment ( $M_o$ ), (2) the corner frequency of the amplitude spectrum ( $f_c$ ), (3) the 1-Hz attenuation quality factors ( $Q_o$ ) for all of the paths, and (4) the frequency dependence ( $\eta$ ) of attenuation along the paths. Because the inversion solves for the path attenuation characteristics, little *a priori* information is needed for the analysis. The resulting  $M_o$  and  $f_c$  values are used in conjunction with the  $m_b$  values as seismic discriminants. The populations of earthquakes and explosions have nearly identical relationships between their moments and corner frequencies. For earthquakes, the relationship is  $\log M_o = 16.07 - 2.93 \log f_c$ . For the set of NTS explosions (using an earthquake source model), the relationship is  $\log M_o = 15.87 - 2.76 \log f_c$ . A source discriminant is found, however, through a comparison of the moments and  $m_b$  values. This gives a line,  $\log M_o = 10.20 + 1.16m_b$ , which cleanly separates the earthquake and explosion populations, with earthquakes falling above and explosions below the line. Reliability tests examine the inverse trade-off between moments and  $Q_o$  values. Noise in the  $Lg$  spectra has a limited effect on the scaling relations.

## Introduction

There is current interest in being able to identify small-yield nuclear tests. This creates a significant seismological challenge because of the large number of small earthquakes that occur daily. A large amount of broadband and short-period array digital seismic data, collected by the International Monitoring System (IMS) of the Comprehensive Nuclear Test Ban Treaty (CTBT), needs to be examined in near real-time. Fortunately, the source spectra of explosions and earthquakes have enough differences that they may make such distinctions possible. This article quantifies the differences manifested in one particular phase, the  $Lg$  wave, with the aim of establishing a fast and accurate seismic source discriminant.

The differences between the earthquake and explosion  $Lg$  waveforms are largely due to the differences in the characteristics of their source-time function and spatial source dimensions (Woods and Helmberger, 1997). Explosions are

compact impulsive sources, and compared to earthquakes with a similar release of low-frequency energy, generate greater amounts of high-frequency energy (Walter *et al.*, 1995). In addition, while  $Lg$  energy is primarily from direct shear waves, the  $Lg$  energy from explosions is formed by  $P$ - $SV$  mode conversions and scattering. Therefore, for a given source moment and focal depth, it is anticipated that earthquakes will generate larger  $Lg$  amplitudes than explosions (Serenio *et al.*, 1988). One way that this is evident is in the relationship between the seismic moment,  $M_o$ , and the body wave magnitude,  $m_b$ . Because the  $m_b$  magnitude is obtained from short-period waves, it differs less between earthquakes and explosions than the moment does. The  $Lg$  waves provide a convenient means of obtaining the moment, and combined with an  $m_b$  value obtained from first arrivals, they can provide a source discriminant.

Because the estimates of both  $M_o$  and  $f_c$  are affected by the regional path attenuation,  $Q_{Lg}$ , it is necessary to account for the attenuation in analyses of  $Lg$  spectra. We demonstrate a method of simultaneously extracting estimates of  $M_o$ ,  $f_c$ ,

\*Present address: Department of Geosciences, University of Arizona, Tucson, Arizona.

$Q_o$  ( $Q_{Lg}$  obtained at a frequency of 1 Hz) and  $\eta$  (the frequency dependence of  $Q_{Lg}$ ). These values are found through a standard parameterization of the  $Lg$  spectra and a genetic algorithm optimization to obtain the parameters. Little *a priori* information such as regional velocity and  $Q$  structures is needed, allowing for near real-time applications.

The  $Lg$  wave is the most prominent phase in short-period and broadband regional seismograms. As has long been observed, the phase is robust and stable in its transmission through continental crust (Press and Ewing, 1952; Ewing *et al.*, 1957).  $Lg$  can be thought of both as a superposition of multiply reflected shear waves entirely confined within the crust (Bouchon, 1982; Kennett, 1986), or as a summation of higher-mode surface waves that travel with an average group velocity of 3.5 km/sec (Knopoff *et al.*, 1973; Herrmann and Kijko, 1983; Wang and Herrmann, 1988; Zhang and Lay, 1995). The stability of the  $Lg$  wave amplitudes makes them a good measure of both the magnitude of the seismic source and the anelastic crustal structure along the wave path (Street *et al.*, 1975; Dwyer *et al.*, 1983; Shin and Herrmann, 1987). Fortunately, the source size and path attenuation can be simultaneously extracted from the  $Lg$  amplitudes (Nuttli, 1973, 1986; Sereno *et al.*, 1988; Xie, 1993). Many aspects of the  $Lg$  wave have been studied, including its generation, the formation of its coda of scattered energy, its propagation, and its use as a regional discriminant of seismic source types (Aki, 1969, 1980; Herrmann, 1980; Bouchon, 1982; Singh and Herrmann, 1983; Raouf and Nuttli, 1985; Kennett, 1986; Campillo, 1987; Campillo, 1990; Bennett and Murphy, 1986; Taylor *et al.*, 1988; Jin and Aki, 1988; Nuttli, 1988; Xie and Nuttli, 1988; Xie and Mitchell, 1990a, b; Ou and Herrmann, 1990; Mitchell, 1995; Zhang and Lay, 1995; Walter *et al.*, 1995; Patton and Taylor, 1995).

For this study we examine 15 nuclear explosions from the Nevada Test Site (NTS) and 25 western United States (WUS) earthquakes, all recorded at four stations operated by the Lawrence Livermore National Laboratory (LLNL) (Table 1). We model the events to find the best-fitting values of  $M_o$  and  $f_c$ , and then examine the relationships between  $M_o$ ,  $f_c$ , and the body-wave magnitude ( $m_b$ ) for use as a seismic source discriminant.

### Spectral Representation of $Lg$ Waves

Following the parameterization of Street *et al.* (1975), we define the  $Lg$  amplitude spectrum for the  $i$ th seismogram as

$$A_i(f, \Delta_i) = S(f)G(\Delta_i) \exp\left[\frac{-\pi f \tau_i}{Q_i(f)}\right], \quad (1)$$

where  $f$  is frequency,  $\Delta_i$  is the distance (in km) to the station,  $S(f)$  is the source function,  $G(\Delta_i)$  is the geometrical spreading term,  $\tau_i$  is the travel time, and  $Q_i(f)$  is the  $Lg$  path attenuation.

Table 1  
LLNL Station Locations

Station	Latitude (N)	Longitude (E)
MNV	38.432	-118.154
KNB	37.016	-112.822
LAC	34.390	-116.411
ELK	40.744	-115.240

The geometrical spreading term,  $G(\Delta_i)$ , is expressed as  $(\Delta_o \Delta_i)^{-1/2}$ , where  $\Delta_o$  is an arbitrary reference distance that is chosen here to be 100 km (Street *et al.*, 1975). This makes  $G(\Delta_i) = 0.1 \Delta_i^{-1/2} \text{ km}^{-1/2}$ . The attenuation  $Q_i(f)$  is expressed as a function of frequency by

$$Q_i(f) = Q_{oi} f^\eta \quad (2)$$

where  $Q_o$  is the attenuation at 1 Hz, and  $\eta$  expresses the frequency dependence. While  $Q$  is often assumed to be essentially constant at longer periods, this is not the case at the high frequencies that comprise  $Lg$ , and  $\eta$  is therefore a non-zero positive number. Both  $Q_o$  and  $\eta$  are free parameters in our inversion.

The source function,  $S(f)$ , contains the other two free parameters,  $M_o$  and  $f_c$ . We used the Sereno *et al.* (1988) formulation of a Mueller and Murphy (1971) explosive source model to define the explosive source term as

$$S(f) = \frac{M_o}{4\pi\rho\beta^3} \left[ 1 + (1 - 2B) \frac{f^2}{f_c^2} + B^2 \frac{f^4}{f_c^4} \right]^{-1/2}, \quad (3)$$

where  $B$  estimates the overshoot effect and is formulated by Mueller and Murphy (1971) as  $\alpha^2/4\beta^2$ , where  $\alpha$  and  $\beta$  are the average compressional and shear wave velocities, and  $\rho$  is the average rock density in the source region. The earthquake source term, appropriate for a double couple, is also from Mueller and Murphy (1971) via Sereno *et al.* (1988), but with the overshoot,  $B$ , set equal to zero. This is given as

$$S(f) = \frac{M_o}{4\pi\rho\beta^3} \left[ 1 + \frac{f^2}{f_c^2} \right]^{-1}. \quad (4)$$

At low frequencies both sources approach  $S(f) = M_o/(4\pi\rho\beta^3)$  but they behave differently when frequencies approach and exceed the corner frequency,  $f_c$ . Since the corner frequency is related to the rupture duration (Savage, 1972), we expect lower values of  $f_c$  for larger events, which tend to have longer source durations. For both the explosion and earthquake sources, the amplitudes fall off as  $f^{-2}$  at frequencies higher than the single corner frequency. The theoretical  $Lg$  spectral model, as represented by equations (1)–(4), has the advantage of being a function of a limited number of parameters ( $M_o$ ,  $f_c$ ,  $Q_o$ ,  $\eta$ ), which can be simultaneously solved for by a genetic algorithm.

For our inversion, we use  $\rho = 2.7 \text{ gm/cm}^3$ , and  $\beta =$

3.5 km/sec. The overshoot value is set at 0.75, which is the same value used by Xie (1993). As in Xie (1993), we also assume that site effects are minimal on  $Lg$ , and that the  $Lg$  wave radiation patterns vary only modestly with azimuthal variation (Alexander, 1985).

### Inversion of $Lg$ Spectra

Since our goal is to provide a general, near real-time estimate of source properties based on the spectra of  $Lg$  waves, we wish to rely upon as little *a priori* information as possible. By using a global search method, in this case, a genetic algorithm (GA), we can easily include the attenuation structure as an unknown, avoiding the need of a preexisting regional  $Q$  model. Use of a genetic algorithm also avoids the requirement of linearizing an inherently nonlinear problem. The forward calculation of  $Lg$  spectra depends upon a small number of parameters and is computationally fast, so the inverse problem is well-suited for a global search method.

Genetic algorithms search a bounded model space using operators based upon evolutionary principles, gradually improving an initially random population of candidate models (Goldberg, 1989; Stoffa and Sen, 1991). Versions of this GA have been previously used in applications of waveform modeling for focal mechanism determination (Koper *et al.*, 1999), surface wave inversion for lithospheric structure (Al-eqabi *et al.*, 1997), and determining a radial core structure using  $PKP$  arrival times (Wyssession and Koper, 1996). Further details of this GA can be found in Koper (1998). The improvement of the models is quantified by evaluating an objective function, which assigns a scalar value ( $\sigma$ ), generally referred to as the cost, to each vector of model parameters. The models consist of the values of  $M_0$  and  $f_c$  for each source, as well as  $Q_0$  and  $\eta$  for each source-receiver path. As a result, the number of parameters varies within 4–10, based upon the number of stations reporting data for a given event (1–4). The bounds for these parameters are listed in Table 2. The cost of the models is expressed as the sum of the differences between the observed and computed amplitude spectra

$$\sigma = \sum_{i=1}^N \sum_{f_{\min}}^{f_{\max}} [\ln A_i^{\text{obs}}(f, \Delta_i) - \ln A_i^{\text{comp}}(f, \Delta_i)], \quad (5)$$

where  $N$  is the number of station used (1, 2, 3, or 4),  $A_i^{\text{obs}}$  is the observed data spectrum,  $A_i^{\text{comp}}$  is the computed synthetic spectrum,  $f_{\min}$  and  $f_{\max}$  are the range of frequencies, and  $\Delta$  is the epicentral distance.

For each earthquake and explosion we use a population of 100 models, expressed as the linear concatenation of the binary representations of the model parameters. The models are initially chosen at random from within the parameter ranges shown in Table 2, but are allowed to evolve during the optimization. Limiting the possible bounds on the param-

Table 2  
Inversion Parameter Bounds Used in the Inversion

Parameter	Minimum	Maximum	Increment	Total Possible Values
Log (Seismic Moment)	15	19	0.000122	32.768
Corner frequency for Eqs.	0.30	1.0	0.0225	32
Corner frequency for Explos.	0.40	1.4	0.0322	32
Q at 1 Hz	100.0	350.0	8.0645	32
Frequency dependence	0.1	0.99	0.0287	32

eters is a process similar to the application of damping in a least-squares inversion: it prevents noise in the data from being mapped into unrealistic individual parameter values. These bounds need to be chosen with care, as with the application of damping within inversions. For instance, the upper limit of 350 for possible  $Q_0$  values is in keeping with previous  $Lg$  studies of Basin and Range attenuation, which show values of 300 or less (Singh and Herrmann, 1983; Peseckis and Pomeroy, 1984; Chavez and Priestley, 1986; Nuttli, 1986; Rogers *et al.*, 1987; and Baqer and Mitchell, 1998; Xie and Mitchell, 1990b).

Models are first ranked according to their cost. A process of selection occurs by assigning a fitness value to each model, based upon the cost, that determines the likelihood of the model's survival. A Roulette wheel selection is used, where the models' fitnesses are used to assign them pieces of a unit interval: the best model (lowest cost) receives the largest slot, and the worst model receives the smallest slot. A new set of 100 models is chosen at random from the existing models, using the roulette wheel assignments. In general, multiple copies of the best models survive, but none for the worst models. The best model is always kept, to ensure that an exceptional model is not lost by chance.

The surviving models are then paired off in order of their original costs and reproduce to create the next generation of models. Reproduction occurs by swapping the back halves of the binary strings representing the two models of a pair. The probability of this cross-over occurring is set at 0.9. When crossover occurs, there is a chance that the offspring will be subject to mutation. This is achieved by randomly flipping bits of the model strings with a probability of 0.025. Once a new generation is attained, the process begins again, starting with a ranking of the new models according to their costs. The process is repeated for 100 iterations (generations), although the population of models usually converges to optimal values much sooner. Because GAs are stochastic processes that operate on a finite set of models, the results of a particular search depend upon the specific initial population of models, though usually to a very small degree if the GA parameters are well chosen. In testing the GA process, the full inversion was run in its entirety multiple times using different random number seeds, in order to assess the stability of our solutions. In all cases, the final solutions for the multiple runs were nearly identical, signifying

that we were very close to the actual global minimum in cost reduction.

### Data

The locations of the four LLNL stations used to record our seismograms are given in Table 1. They surround the NTS explosions at distances of 199–412 km, and were 190–1006 km away from the 25 WUS earthquakes analyzed (Fig. 1). The LLNL instruments have a velocity response that is flat in the range of 0.07–5.0 Hz (Taylor, 1993), which contains the frequencies we use here. The 15 explosions had magnitudes of  $4.4 \leq m_b \leq 5.7$ , and the 25 earthquakes had  $4.8 \leq m_b \leq 6.0$  (Table 3). The depths of the earthquakes ranged from 0 to 21 km.

The  $L_g$  waves were taken from the digital vertical components and were isolated in a manner similar to Chael (1987) and Atkinson and Mereu (1992) to obtain stable estimates of the  $L_g$  spectra. Future availability of three-component data would allow this kind of analysis to incorporate the horizontal components, which may be more appropriate for the  $L_g$  phase. A time window was selected that corresponds to  $L_g$  arrivals with group velocities between roughly 2.9 and 3.7 km/sec (the exact upper and lower bounds depended upon the quality of the seismic record). As a result, the window length increased with the earthquake-station distance to account for the dispersion of  $L_g$ . The length of the window ranged from 45.3 sec long (for an epicentral distance of 1011.7 km), to 12.7 sec long (for an epicentral distance of 195.7 km). This window was then divided into many smaller segments, each having a 50% overlap with adjacent segments and 5% cosine tapers at the ends. The segment lengths, from 4 to 10 sec, varied with event size, epicentral distance, and sampling rate.

The spectrum of each segment  $d_i(f)$  was computed separately, and the multiple spectra were then summed according to Atkinson and Mereu (1992), represented by

$$A(f) = \left[ \sum_{i=1}^n d_i^2(f) \frac{T}{nt} \right]^{1/2}, \quad (6)$$

where  $A(f)$  is the summed spectrum,  $T$  the duration of the total  $L_g$  window,  $n$  the number of data segments, and  $t$  the duration of the window segments. The summed spectrum  $A(f)$  was then smoothed across frequencies using a moving average with a window of constant logarithmic frequency (B. Herrmann, personal commun.). This smoothed spectrum  $\bar{A}(\bar{f}_i)$  is computed at a discrete set of frequencies,  $\bar{f}_i = 10^{(-0.5 + 0.05i)}$ , where  $i = 0, 30$ . The smoothing at each frequency  $\bar{f}_i$  is carried out as

$$\bar{A}(\bar{f}_i) = \frac{1}{j_{\text{up}}(i) - j_{\text{low}}(i) + 1} \sum_{j=j_{\text{low}}(i)}^{j_{\text{up}}(i)} A(f_j) \quad \text{with} \quad (7)$$

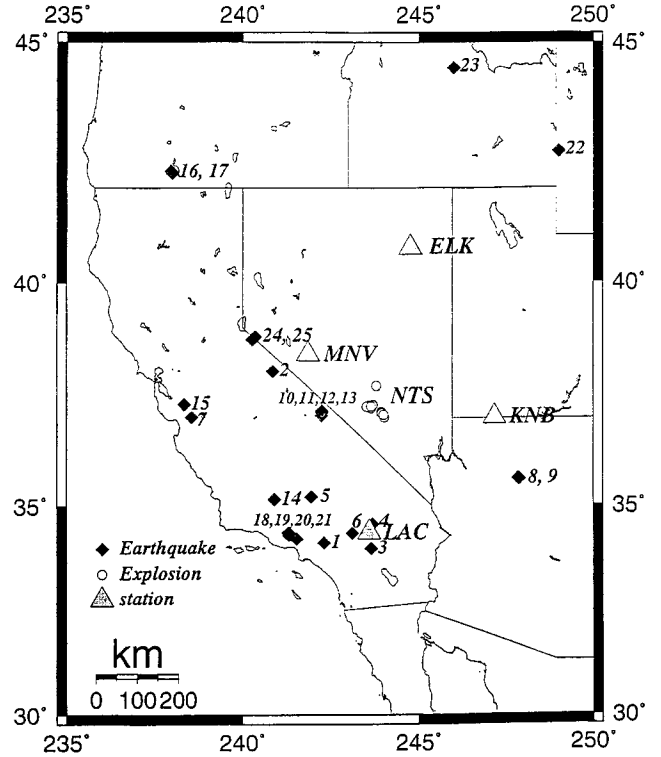


Figure 1. A map of the western United States showing earthquakes (diamonds, accompanied by identifying numbers), Nevada test site (NTS) explosions (open circles) and locations of the four broadband seismic stations (triangles) used in this study.

$$j_{\text{up}}(i) = \text{nint}[10^{(-0.45 + 0.05i)/df} + 1] \quad \text{and}$$

$$j_{\text{low}}(i) = \text{nint}[10^{(-0.55 + 0.05i)/df} + 1],$$

where  $df$  is the discrete frequency interval of the summed spectrum  $A(f)$ , and  $j_{\text{up}}(i)$  and  $j_{\text{low}}(i)$  are the upper and lower indices that determine the moving spectral window for smoothing. The length of the smoothed spectral window used for further analysis varied with the length of the usable individual data segment spectra, which were functions of the length of the original  $L_g$  time window.

For each  $L_g$  window, a noise spectrum was obtained from a single segment that preceded the  $P$  wave. This noise spectrum was processed in a fashion similar to the signal segments, normalized to the same duration as the signal, and then subtracted from the signal power. The noise was subtracted in the same manner as Atkinson and Mereu (1992), through

$$A'(f_d) = [\bar{A}^2(f_d) - N^2(f_d)]^{1/2}, \quad (8)$$

where  $N(f_d)$ ,  $\bar{A}(f_d)$  and  $A'(\omega_i)$  are the spectra of the noise, smoothed data, and the noise-corrected data signals, respectively. Using a pre- $P$  window for determining the noise spectrum, as opposed to the pre- $L_g$  window, is commonly done with  $L_g$  studies (Serenio *et al.*, 1988; Xie, 1993; Xie *et al.*,

Table 3  
Western United States Earthquakes and Nevada Test Site Explosions Used for the Determination of Source Parameters

Event	Date (m d y)	Origin Time (h:m:s)	Latitude	Longitude	Depth (km)	$m_b$ (mb)	Number of Stations Used
Western United States Earthquakes							
(1) Upland, CA	2 28 90	23:43:36.60	34.140	-117.700	5	5.5	2
(2) Lee Vining, CA	10 24 90	06:15:12.70	38.047	-119.157	12	5.4	2
(3) Landers, CA	6 30 92	14:38:11.59	34.004	-116.361	0	5.1	2
(4) Landers, CA	7 5 92	21:18:27.09	34.583	-116.319	0	5.3	2
(5) Garlock, CA	7 11 92	18:14:16.15	35.210	-118.066	10	5.3	2
(6) Big Bear, CA	12 4 92	02:08:57.50	34.369	-116.897	3	5.3	3
(7) Gilroy, CA	1 16 93	06:29:34.90	37.025	-121.458	5	4.8	3
(8) Cataract Creek, AZ	4 25 93	09:29:50.30	35.624	-112.147	10	5.0	3
(9) Cataract Creek, AZ	4 29 93	08:21:00.81	35.611	-112.112	10	5.5	3
(10) Eureka Valley, CA	5 17 93	23:20:49.22	37.171	-117.775	6	6.0	2
(11) Eureka Valley, CA	5 18 93	01:03:06.43	37.152	-117.762	2	4.6	2
(12) Eureka Valley, CA	5 18 93	23:48:53.90	37.064	-117.777	3	5.0	2
(13) Eureka Valley, CA	5 19 93	14:13:22.58	37.137	-117.768	0	4.9	2
(14) Bakersfield, CA	5 28 93	04:47:40.60	35.149	-119.104	21	4.6	1
(15) Alum Rock, CA	8 11 93	22:33:04.00	37.313	-121.675	9	4.6	4
(16) Klamath Falls, OR	9 21 93	03:28:55.42	42.314	-122.012	10	5.7	4
(17) Klamath Falls, OR	9 21 93	05:45:33.75	42.358	-122.045	5	5.6	4
(18) Northridge, CA	1 17 94	23:33:30.69	34.326	-118.698	9	5.7	3
(19) Northridge, CA	1 18 94	00:43:08.79	34.377	-118.698	11	5.4	3
(20) Northridge, CA	1 19 94	21:09:28.59	34.379	-118.711	14	5.1	2
(21) Northridge, CA	3 20 94	21:20:12.20	34.231	-118.475	13	5.2	2
(22) Drainey Peak, ID	2 3 94	09:05:04.20	42.762	-110.976	7	5.4	3
(23) Near Borah Peak, ID	6 7 94	13:30:03.47	44.493	-114.003	5	4.8	2
(24) Double Springs Flat, NV	9 12 94	12:23:43.20	38.819	-119.652	14	5.4	3
(25) Double Springs Flat, NV	9 12 94	23:57:09.84	38.759	-119.744	0	4.9	3
Nevada Test Site Explosions							
(1) Schellbourne	5 13 88	15:35:00.11	37.124	-116.072	—	4.8	3
(2) Alamo	7 7 88	15:05:30.07	37.252	-116.377	—	5.6	3
(3) Kearsarge	8 17 88	17:00:00.09	37.297	-116.307	—	5.5	4
(4) Texarkana	2 10 89	20:30:00.00	37.077	-116.000	—	5.2	3
(5) Ingot	3 9 89	14:05:00.00	37.143	-116.067	—	5.0	3
(6) Contact	6 22 89	21:15:00.00	37.283	-116.412	—	5.3	2
(7) Amarillo	6 27 89	15:30:00.00	37.275	-116.354	—	4.9	3
(8) Hornitos	10 31 89	15:30:00.00	37.263	-116.490	—	5.7	4
(9) Metropolis	3 10 90	16:00:00.00	37.112	-116.055	—	5.0	4
(10) Bullion	5 13 90	15:34:59.99	37.262	-116.420	—	5.7	4
(11) Mineral Quarry	7 25 90	15:00:00.00	37.720	-116.210	—	4.7	4
(12) Houston	11 14 90	19:17:00.07	37.227	-116.371	—	5.4	3
(13) Bexar	4 4 91	15:34:59.99	37.296	-116.313	—	5.6	4
(14) Junction	3 26 92	16:30:00.99	37.272	-116.360	—	5.5	3
(15) Divider	9 23 92	15:04:00.00	37.021	-115.988	—	4.4	2

The origin times and locations are from the U.S. Geological Survey's Preliminary Determination of Epicenters.  $m_b$  values are obtained from the USGS National Earthquake Information Center at web site, <http://www.neic.cr.usgs.gov/neis/epic/epic.html>

1996; Cong *et al.*, 1996). A pre- $Lg$  window contains the  $S_n$  coda, and it therefore produces an overestimation of the noise present throughout the  $Lg$  signal, and the use of a pre- $Lg$  noise window may overestimate the high-frequency part of the  $Lg$  spectrum due to the persistence of the  $P$  coda throughout the signal (Boore and Atkinson, 1992).

The result of the multisegment technique is an  $Lg$  amplitude spectrum that is more stable than the spectrum obtained from a simple Fourier transform of the whole  $Lg$  window. By stable, we mean that the spectrum amplitudes are less variable over small changes in frequency and, therefore, more similar to the theoretical spectra to which they will be

compared. Part of this stability is due to the windowing technique, where summing several spectra smooths out the spectral peaks that result from a single window, and some of the stability comes from the spectral smoothing done with the constant-logarithmic-window moving average. We get stable  $Lg$  amplitudes between 0.316 Hz at the lower end and 5 to 10 Hz at the higher end for both earthquakes and explosions. It is important that we have good  $Lg$  signals at frequencies that are low enough to be able to constrain the low-frequency moment and corner frequency estimates. Examples of the multisegment technique are shown for an earthquake and an explosion in Figures 2 and 3. These two

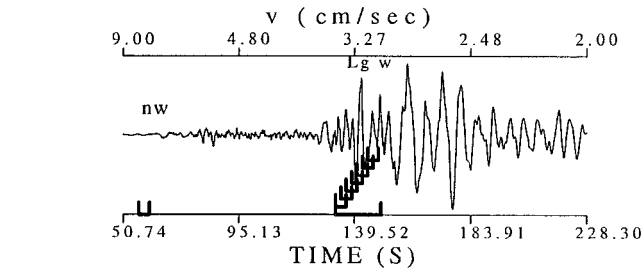


Figure 2. A seismogram recorded at station ELK from an earthquake in Eureka Valley, California 18 May 1993, 23 hr showing the  $L_g$  wave time series and its isolated spectrum (squares). The large bracket shows the extent of the  $L_g$  wave window, and the smaller brackets show the individual segments used in analyzing the  $L_g$  spectrum. The amplitude spectra of these segments  $d_i(f)$  are shown with the thin lines, and the thick line is the summed spectrum  $A(f)$  of equation (6). The squares  $[\hat{A}(f_d)]$  of equation (7) are smoothed spectral amplitudes computed at discrete frequencies. The noise window is labeled as nw, and its amplitude is shown with the dashed line.

events were selected because both have comparable epicentral distances to the station ELK of LLNL. The seismogram are shown, displaying the times of the multiple signal segments as well as the noise segment. The multiple thin lines are the spectra of the separate segments, the solid line is the summed spectrum (equation 6) of the individual spectra. The squares show the smoothed  $L_g$  spectrum (equation 7), and the dashed line shows the noise spectrum. Note that none of the individual spectra (thin lines) dominates the final smoothed spectrum (squares).

## Results

The GA inversion finds the set of parameters ( $M_0$ ,  $f_c$ ,  $Q_0$ ,  $\eta$ ) that best fits the spectral amplitude curves just dis-

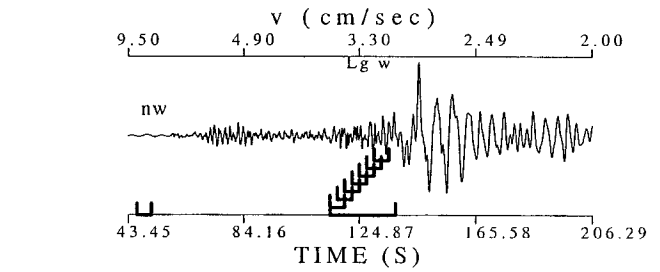


Figure 3. Same as Figure 2, but for an NTS explosion (Texarkana, 10 February 1989) recorded at station ELK.

cussed. For the earthquake and explosion examples shown in Figures 2 and 3, the fits of the resulting models to the data are shown in Figures 4 and 5. The results of the modeling for all of the earthquakes and explosions are shown in Tables 4 and 5 and in the following figures. The values for the earthquake-station path attenuation were very internally consistent. They suggest a gradual transition from lower attenuation ( $Q_0 = 300-320$ ) at the northeastern part of our region of study (northeastern Nevada), to greater attenuation ( $Q_0 \leq 260$ ) at the southwestern part of our study area (southern California). These results will be presented in a subsequent publication.

Figure 6 shows the log-log plot of the observed moments versus corner frequencies for the set of 25 WUS earthquakes processed using a theoretical earthquake source (double-couple). Events of larger moment usually have lower corner frequencies, and the two are expected to be related by a scaling law that takes the form of

$$M_0 = \text{constant} \times f_c^x, \quad (9)$$

where  $x$  is a negative constant that is often in the range of  $-2$  to  $-3$  (Aki, 1967; Nuttli, 1983). According to equation

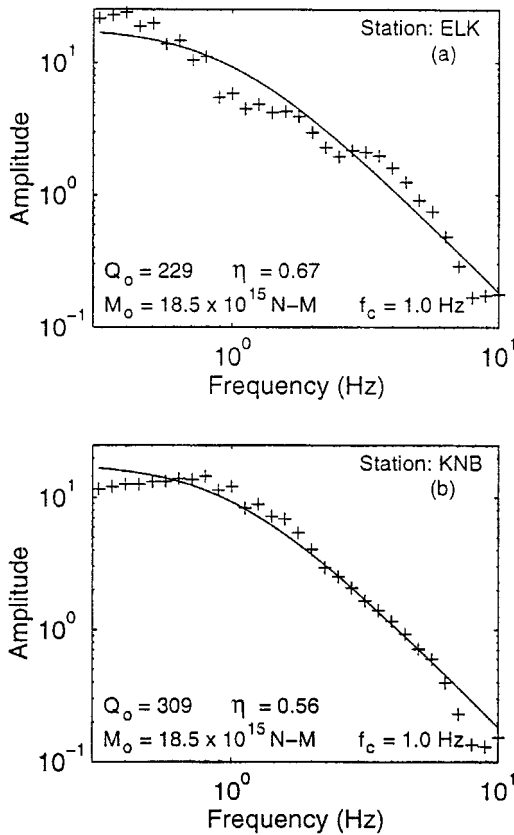


Figure 4. Examples of fits between observed (plus signs) and predicted (solid line)  $Lg$  source spectra for the Eureka Valley, California, earthquake depicted in Figure 2, shown at the two recording stations. The predicted source spectrum is calculated using the optimal source model parameters,  $M_o$  and  $f_c$  (Table 4), and path attenuation parameters,  $Q_o$  and  $\eta$ , found through a genetic algorithm search and shown inside each panel. The observed  $Lg$  source spectra (plus signs) are obtained by correcting for the instrument response, geometrical spreading, and path attenuation, and by using the method described in Figure 2 of smoothing a summed set of individual  $Lg$  subsection spectra.

(9), the log values in Figure 6 should lie along a straight line, whose slope is the scaling constant  $x$ .

The slope of the line that best fits the log-log values in Figure 6 is computed using a least-squares linear regression through the points, minimizing only the log  $M_o$  values. This is done to provide a comparison with previous studies, which have used the same method. The result is

$$\log M_o = 16.07(\pm 0.54) - 2.93(\pm 0.85) \log f_c, \quad (10)$$

and the correlation coefficient is  $R = -0.58$ . The uncertainties given are  $1 \sigma$  standard deviations in the slope and intercept. The scaling relation of  $-2.93$  is different than the value of  $-1.97$  obtained by Mitchell *et al.* (1997) for the

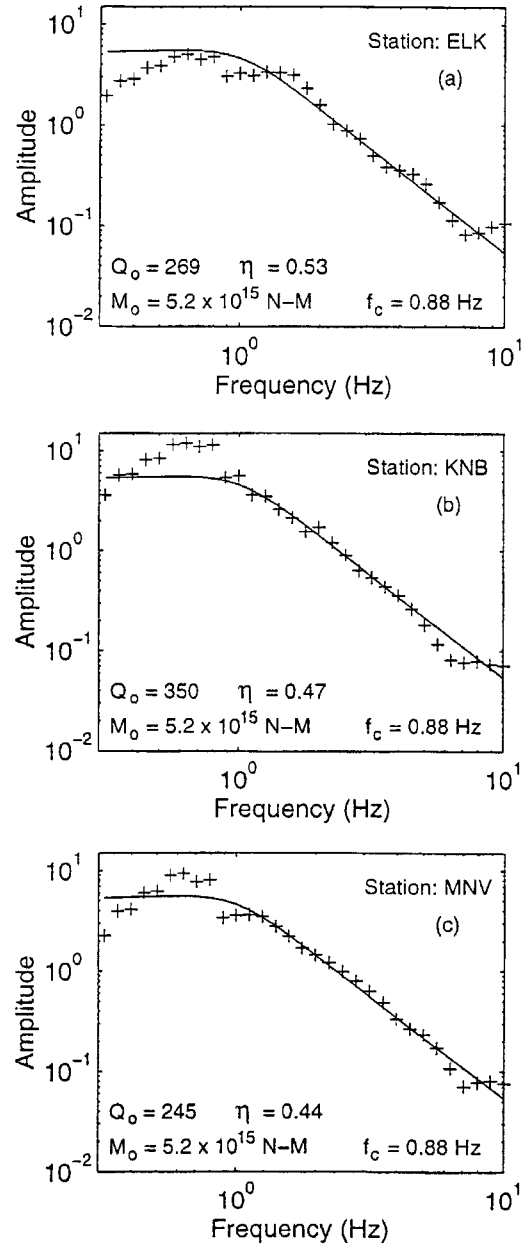


Figure 5. Same as Figure 4, but for the three stations that recorded the Texarkana NTS explosion.

eastern United States from 31 earthquakes, but is closer to that obtained by Cong *et al.* (1996) for 51 earthquakes in central Asia ( $-3.56$ ).

Figure 7 shows a log-log plot of the GA-obtained  $M_o$  values compared with the  $m_b$  values, also for the set of WUS earthquakes using an earthquake source. The linear regression yields

$$\log M_o = 9.72(\pm 0.84) + 1.37(\pm 0.15)m_b, \quad (11)$$

and the correlation coefficient is  $R = 0.88$ .

Table 4  
Source Parameters of WUS Earthquakes

Earthquake	$M_0 \times 10^{15}$ (N m)			$f_c$ (Hz)	
	Earthquake Source		Published	Earthquake Source	
	Noise Correction	No Noise Correction	Moments	Noise Correction	No Noise Correction
(1) Upland, CA	266.0	178.0	250.0*	0.37	0.50
(2) Lee Vining, CA	95.5	89.7	77.0*	0.39	0.48
(3) Landers, CA	34.4	55.4	6.7*	0.46	0.39
(4) Landers, CA	154.0	160.0	—	0.66	0.48
(5) Garlock, CA	44.4	47.2	—	0.53	0.55
(6) Big Bear, CA	38.5	54.3	73.0†	0.46	0.48
(7) Gilroy, CA	17.5	17.2	38.0†	0.50	0.50
(8) Cataract Creek, AZ	14.1	14.7	16.0†	0.62	0.80
(9) Cataract Creek, AZ	72.7	83.8	100.0†	0.59	0.50
(10) Eureka Valley, CA	571.0	583.0	1400.0†	0.41	0.40
(11) Eureka Valley, CA	15.5	15.1	—	0.64	0.82
(12) Eureka Valley, CA	24.3	25.6	—	1.00	1.00
(13) Eureka Valley, CA	18.5	18.1	—	1.00	0.93
(14) Bakersfield, CA	16.2	16.2	15.0†	0.64	0.64
(15) Alum Rock, CA	15.3	16.0	18.0†	0.53	0.53
(16) Klamath Falls, OR	605.0	227.0	1100.0†	0.44	0.68
(17) Klamath Falls, OR	589.0	489.0	1100.0†	0.50	0.55
(18) Northridge, CA	931.0	486.0	870.0†	0.32	0.53
(19) Northridge, CA	59.3	62.0	—	0.62	0.66
(20) Northridge, CA	70.8	83.5	—	0.44	0.44
(21) Northridge, CA	76.9	55.5	—	0.59	0.68
(22) Drainey Peak, ID	309.0	310.0	420.0*	0.57	0.50
(23) Near Borah Peak, ID	42.5	38.3	—	0.62	0.64
(24) Double Springs Flat, NV	249.0	231.0	—	0.48	0.50
(25) Double Springs Flat, NV	28.3	29.7	—	0.53	0.50

\*Moments from Dreger and Helmberger (1993).

†Moments from Ritsema and Lay (1995).

Table 5  
Source Parameters of NTS Explosions

Explosion	$M_0 \times 10^{15}$ (N m)				$f_c$ (Hz)		
	Explosion Source	Earthquake Source		Published Moments	Explosion Source	Earthquake Source	
		Noise Correction	Noise Correction			No Noise Correction	Noise Correction
(1) Schellbourne	2.29	3.21	2.53	3.0	0.88	0.88	1.01
(2) Alamo	11.6	16.0	15.1	23.0	0.98	1.14	1.27
(3) Kearsarge	9.12	10.0	8.77	18.0	0.82	0.88	1.11
(4) Texarkana	5.2	7.15	6.8	8.1	0.88	1.17	1.17
(5) Ingot	4.67	6.31	6.12	—	0.79	0.82	0.88
(6) Contact	17.3	16.1	12.5	21.0	0.69	0.88	0.88
(7) Amarillo	2.44	3.15	3.11	1.5	0.88	1.17	1.37
(8) Hornitos	16.8	34.2	35.0	—	0.72	0.66	0.69
(9) Metropolis	5.97	7.62	7.45	—	0.75	0.92	0.98
(10) Bullion	24.5	33.6	30.4	—	0.66	0.85	0.92
(11) Mineral Quarry	1.31	1.35	1.58	—	0.66	1.08	1.14
(12) Houston	4.58	6.7	5.1	—	0.88	1.14	1.40
(13) Bexar	10.9	11.8	11.4	24.0	0.63	0.88	0.95
(14) Junction	7.5	11.5	13.4	—	0.85	1.30	1.08
(15) Divide	0.748	1.28	1.34	1.7,* 0.19†	1.30	1.40	1.40

\*From Zhao and Helmberger (1996).

†From Woods *et al.* (1993).

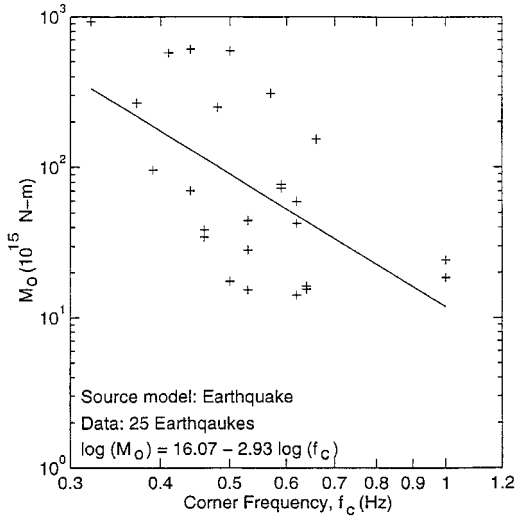


Figure 6. A logarithmic plot of  $f_c$  versus  $M_0$  obtained from the  $Lg$  spectra of 25 earthquakes in the western United States. The solid line is the least-squares regression, which gives a slope of  $-2.93$ . An earthquakes source model is assumed in obtaining the source parameters for these earthquakes.

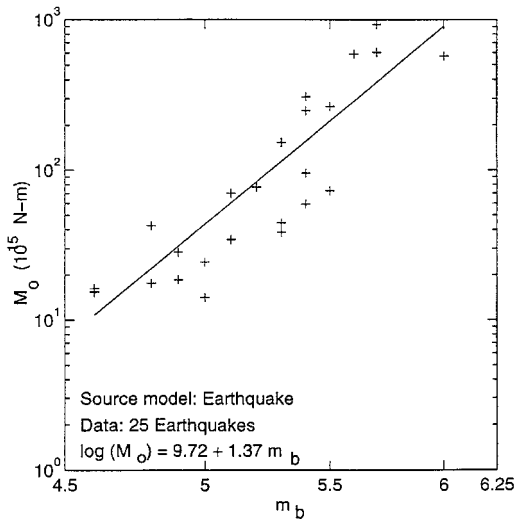


Figure 7. A logarithmic plot of  $M_0$  versus  $m_b$  obtained from the  $Lg$  spectra of the western United States earthquakes. The  $M_0$  values are obtained by fitting the  $Lg$  spectra using an earthquake source (double couple) model. The  $m_b$  values are obtained from published sources. The solid line is the least-squares regression, which gives a slope of  $1.37$ .

Figures 8 and 9 show results equivalent to 6 and 7, but for the 15 NTS nuclear explosions. Modeling is done using values computed for explosion sources. For the log-log relationship between  $M_0$  and  $f_c$ , the linear regression gives

$$\log M_0 = 15.48(\pm 0.40) - 2.98(\pm 1.22) \log f_c, \quad (12)$$

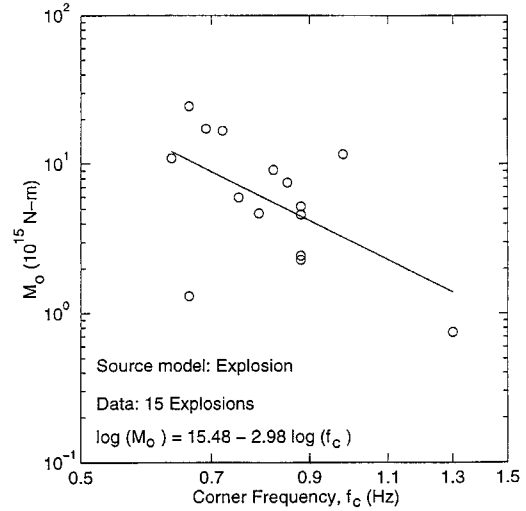


Figure 8. Same as Figure 6, but for the 15 NTS explosions, modeled with an explosion source. The slope is  $-2.98$ .

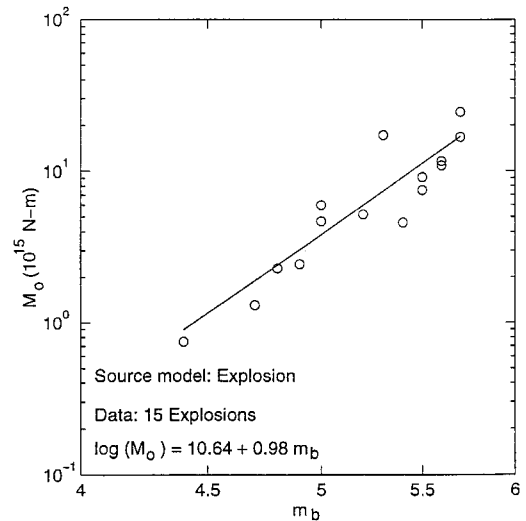


Figure 9. Same as Figure 7, but for the 15 NTS explosions, modeled with an explosion source. The slope is  $0.98$ .

with a correlation coefficient of  $-0.56$ . The scaling parameter of  $-2.98$  does not differ significantly from the  $-3.83$  value obtained by Xie *et al.* (1996) for 20 nuclear explosions in central Asia (also computed with an explosion source).

For the comparison between computed  $M_0$  values and bulletin  $m_b$  values, shown in Figure 9, the linear regression gives

$$\log M_0 = 10.64(\pm 0.64) + 0.98(\pm 0.12)m_b, \quad (13)$$

with a correlation coefficient of  $R = 0.92$ .

There is an obvious flaw with the previous two figures

if the aim is to determine whether a source is an earthquake or an explosion: we do not know *a priori* whether to use an explosion or earthquake source. As there are many more global earthquakes than nuclear tests, we shall assume an earthquake source for all events to see if the two populations separate. While we can expect to do a less satisfactory job of fitting the explosion data if we use an earthquake source, what we gain is much more important: the ability to use the analysis as a straight-forward discriminant between earthquake and explosion data. Using earthquake sources for the computation of the explosions (Fig. 10), the linear regression between the  $\log M_0$  and  $\log f_c$  values yields

$$\log M_0 = 15.87(\pm 0.38) - 2.76(\pm 1.11) \log f_c, \quad (14)$$

with a correlation coefficient of  $-0.56$  (essentially unchanged from the value of  $-0.58$  obtained with the explosion source). The important difference between using the earthquake and explosion sources for computing the explosion parameters is that the earthquake source provides larger  $M_0$  and  $f_c$  values.

The  $\log M_0$  vs.  $\log f_c$  slope of the explosions with an explosion source hardly differed from that of the earthquakes ( $-2.98$  compared to  $-2.93$ ), and this is also true for the explosion parameters computed using an earthquake source ( $-2.76$ ) (Fig. 11). This analysis reveals no systematic difference between the populations of earthquakes and explosions: the moments scale continuously across the two populations with respect to the corner frequencies. Any single explosion could easily be considered part of the earthquake population.

A method of source discrimination can be found, however, by comparing moments and body-wave magnitudes. When the 15 NTS explosions are analyzed with earthquake sources, the resulting linear regression gives

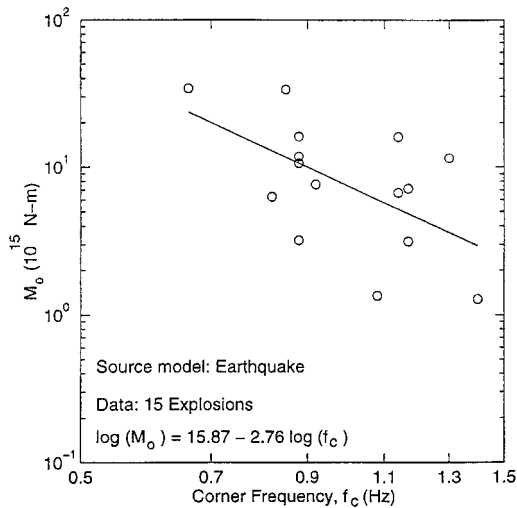


Figure 10. Same as Figure 6, but for the NTS explosions, now modeled with an earthquake source model.

$$\log M_0 = 10.70(\pm 0.61) + 0.99(\pm 0.11)m_b, \quad (15)$$

with a high correlation coefficient of  $R = 0.93$ .

Plotting the  $Lg$ -derived  $\log M_0$  and  $m_b$  values for both earthquakes and explosions together (Fig. 12), it is clear that a strong means of discrimination exists. The fields for the

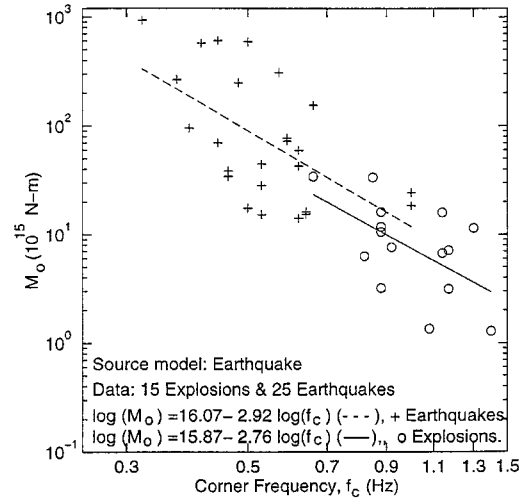


Figure 11. Comparison between the moments and corner frequencies for the populations of explosions (circles) and earthquakes (crosses) studied here. Both are computed using the earthquake source model. The earthquakes and explosions have nearly identical slopes for the relations between  $\log M_0$  and  $\log f_c$ , making it impossible to distinguish the source mechanism of an individual event on this basis.

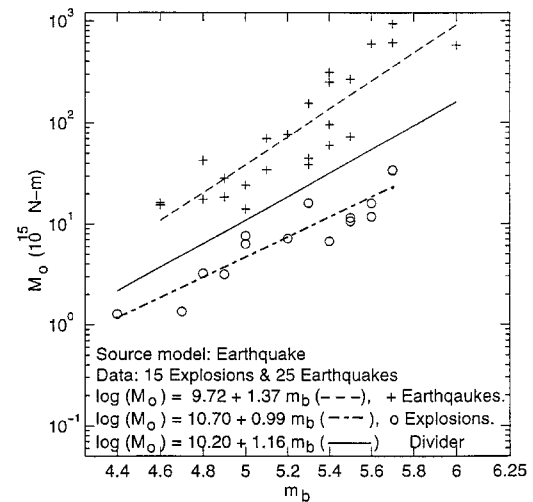


Figure 12. Comparison of the  $Lg$  seismic moments and  $m_b$  magnitudes for the earthquakes (pluses) and explosions (circles) used in this study. Both are modeled with earthquake sources. There is a clear separation between the two populations, represented by the solid line defined in equation (16), which lies nearly halfway between the separate linear fits to the earthquakes and explosions.

earthquake and explosion populations separate into two distinct groups. We define a line that is nearly half-way between the two lines for earthquakes and explosions:

$$\log M_o = 10.20 + 1.16m_b, \quad (16)$$

that separates the two populations. Values above this line are earthquakes, and values below this line are explosions. This kind of discriminant has been demonstrated before by Woods *et al.* (1993) and Patton and Walter (1993). Woods *et al.* (1993) compiled moment values for 299 earthquakes and 178 explosions and plotted them versus the local magnitude,  $M_L$ , values. They found two well-separated populations with respect to source type. This separation is attributed to the different frequencies of the measurements, as  $M_L$  is measured at 1 Hz and the moments are determined at longer periods. The impulsive source of the explosions is less efficient at generating low-frequency waves. Patton and Walter (1993) developed relations between  $M_o$  and  $m_b$  for  $P_n$  waves taken from NTS explosions and U.S. earthquakes. They found the  $\log M_o$  vs.  $m_b$  ( $P_n$ ) slope of the earthquakes (1.12) to be higher than that of the explosions (1.02), while the intercept of the earthquakes (9.55) was lower than that of the explosions (11.27). We observe similar differences in our study. Patton and Walter (1993) preassumed the source type (using explosion sources for explosions) and found an excellent separation between the earthquake and explosion populations, attributing this separation to the combined contributions from different radiation patterns, material properties, and apparent source stress drops. Other studies have also found separations of earthquake and explosion populations in plots of  $M_s$  and  $m_b$  (i.e., Sykes and Evernden, 1982; Taylor *et al.*, 1986).

### Reliability Tests

The separation of the earthquakes and explosions on a plot of  $\log M_o(Lg)$  vs.  $m_b$ , shown in Figure 12, is significant, but it is important to examine the robustness of this result. We are not so concerned with obtaining the most accurate measurements of the moments of the sources, as this would be better found using an analysis that incorporated other seismic phases to use as much of the full seismogram as possible. Rather, we want to make sure that the  $Lg$  wave provides a strong discriminant between explosive and double-couple mechanisms.

One possible source of bias is our attempt to extract signal from noise by subtracting out the power of a sample pre- $P$ -wave noise segment. To check this, we carried out the analysis for the earthquakes and explosions (with earthquake sources) without the noise reduction. We found that for the earthquakes, omitting the noise reduction changed the  $\log M_o$  vs.  $f_c$  slope from  $-2.93$  to  $-2.39$  and intercept from 16.07 to 16.26, and the  $\log M_o$  vs.  $m_b$  slope from 1.37 to 1.24 and intercept from 9.72 to 10.35. For the explosions (with the assumed earthquake source mechanisms), omitting

the noise reduction changed the  $\log M_o$  vs.  $f_c$  slope from  $-2.76$  to  $-3.00$  and intercept from 15.87 to 15.94, and the  $\log M_o$  vs.  $m_b$  slope from 0.99 to 0.97 and intercept from 10.70 to 10.83. There was no systematic change to the moment values through the removal of the noise correction, as seen in Tables 4 and 5. Because spectral noise levels were typically one to two orders of magnitude smaller than the signal spectra, the application of the noise correction in equation 8, involving the difference of the squares of the signal and noise amplitudes, was not significant. The moment values changed slightly when the inversions were run without the noise corrections, but these changes were due to trade-offs with the other free parameters. For example, whenever the moment increased, there was almost always a corresponding decrease in the corner frequency. These variations are an indication of the expected deviations of the GA-derived moment values.

More importantly, omitting the incorporation of the noise reduction does not alter the separation of the earthquakes and explosions on a  $\log M_o(Lg)$  vs.  $m_b$  plot. There is still a clear separation between the earthquake and explosion fields. The same line (equation 16), is still viable as a source delimiter between the earthquakes and explosions.

Another concern is that there might be a systematic trade-off between the seismic moment and attenuation constant. To investigate this trade-off between  $Q_o$  and  $M_o$ , we carried out a test for examples of an earthquake (7 November 1992, Garlock Fault) and an explosion (7 July 1988, Alamo). The  $f_c$  and  $\eta$  values from the best solutions were held constant, and the inversion was rerun for a range of  $Q_o$  values. Figure 13a shows the range of  $M_o$  values (crosses) that result when  $Q_o$  is constrained at values from 100 to 700. The circle shows the original best solution for the two seismograms available (they both have the same  $Q_o$  value: 330). Figure 13c shows the change in cost for this experiment. The optimal solution sits at the bottom of a narrow cost well, with a cost of 6.0. Increasing the cost of the fit by 50%, which represents a significant degradation of the solution, would signify a possible  $Q_o$  range of 255 to 450. This would also signify a range for  $M_o$  of  $81 \times 10^{15}$  to  $26 \times 10^{15}$  N m. This would not move the  $\log M_o$  value in Figure 13 a significant amount.  $M_o$  changes rapidly with respect to  $Q_o$  when  $Q_o$  has low values (Fig. 13a), but the cost rises dramatically at this range (Figure 13c), so this is not likely. The cost rises more slowly for increasing values of  $Q_o$ , but the trade-off with  $M_o$  is less significant for high  $Q_o$ . The result is that unrealistic values of  $Q_o$  are needed to significantly affect our  $M_o$  values, and the high cost of these solutions prevents them from influencing our results. Figures 13b and 13d show the same analysis for the Alamo nuclear test. In this case there are three recording stations, shown at their optimal individual earthquake-station path  $Q_o$  values as circles. Because we constrain all three paths to have the same  $Q_o$  values for our trade-off tests, shown as crosses, the cost values are always higher than the optimal solution. However, the result is the same as for the Garlock earthquake. Large changes in  $Q_o$  are

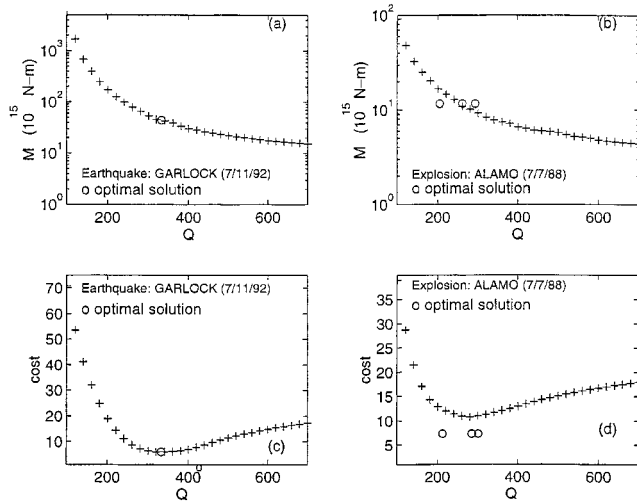


Figure 13. Demonstration of the trade-off between  $M_o$  and  $Q_o$  that results during the GA inversion, shown for an earthquake (Garlock, 7 November 1992) in (a) and (c), and an explosion (Alamo, 7 July 1988) in (b) and (d). The trade-offs are shown in (a) and (b), with circles showing the original optimum values and crosses showing the moments that result when all earthquake-station path  $Q$  values are constrained at a series of values. The costs of these test runs are shown in (c) and (d). The value of the computed moment cannot change greatly without significant increase in the cost, or misfit, of the solution.

needed to significantly change  $M_o$ , but such values are precluded by their high costs. Tests of the trade-off between the moment and the corner frequency showed a very similar relationship. Decreasing  $f_c$  resulted in an increase in  $M_o$ , and increasing  $f_c$  resulted in a decrease in  $M_o$ , though significant increases in either were accompanied by unreasonably high increases in the cost of the solution.

### Conclusions

With further testing,  $Lg$  waves may be used to provide a reliable real-time discriminant between earthquake and explosion sources. If continental paths are available and  $m_b$  values are obtained, then the inversion of the  $Lg$  amplitude spectra provides estimates of the seismic moment, which aids in the source discrimination of an individual seismic event.

We have developed a method of analysis where the event  $Lg$  amplitude spectrum is a function of a small number of independent variables: the seismic moment ( $M_o$ ) and corner frequency ( $f_c$ ) of the seismic event, and the average path attenuation at 1 Hz ( $Q_o$ ) and attenuation frequency dependence ( $\eta$ ) for all of the source-station paths. Because these four parameters interact in a very nonlinear way, a genetic algorithm is used to search efficiently the multiparameter space to obtain optimum models. The inversion simultaneously obtains the average  $Q$  properties for the  $Lg$  wave

paths, so little *a priori* regional information is required. The  $M_o$  estimates are subject to trade-offs with  $Q_o$ , but this effect is too small to invalidate the  $Lg$  moment as a means of source discrimination.

We have applied this method of analysis to 25 shallow western U.S. earthquakes and 15 nuclear tests at the NTS. All seismic records used are from four identical seismometers operated by the Lawrence Livermore National Laboratory in order to help reduce receiver site and instrument biases. As populations, there are no significant systematic differences between the trends of  $f_c$  versus  $M_o$  plots for the earthquakes and explosions. A linear fit to the distribution of earthquake  $\log M_o$  and  $\log f_c$  has a slope of  $-2.93$ . The linear fit to the same distribution of explosion values has a slope of  $-2.76$ . If an appropriate explosive source is used in the  $Lg$  source description for the population of explosions, then the linear slope of the  $\log M_o$  vs.  $f_c$  values becomes  $-2.98$ . None of these slopes are significantly different than the others. The source type of a distinct regional population of events could not be determined using this discriminant.

If the  $m_b$  value is available, however, then a means of discriminating earthquakes from explosions is provided by the  $Lg$ -derived seismic moments ( $M_o$ ). A plot of the moments and the  $m_b$  values results in a distinct separation of the earthquake and explosion populations. This separation can be quantified by a line, equation (16), that is nearly half-way between the best-fit lines that model the earthquake and explosion data separately. For a given  $m_b$ , the earthquake moments are about an order of magnitude larger than the explosion moments.

### Acknowledgments

We thank William Walter for providing the set of LLNL seismograms, Robert B. Hermann for providing us with programs for isolating the  $Lg$  spectra, and Patrick Shore for computer support. This work was supported by an NSF Presidential Faculty Fellowship (EAR-9629018) and the David and Lucile Packard Foundation.

### References

- Aki, K. (1967). Scaling law of seismic spectrum. *J. Geophys. Res.* **72**, 1217–1231.
- Aki, K. (1969). Analysis of the seismic coda of local earthquakes as scattered waves. *J. Geophys. Res.* **74**, 615–631.
- Aki, K. (1980). Scattering and attenuation of shear waves in the lithosphere. *J. Geophys. Res.* **85**, 6496–6504.
- Al-eqabi, G. I., K. D. Koper, M. E. Wyssession, P. J. Shore, K. M. Fischer, and T. J. Clarke (1997). Lithospheric cross-section across the northeastern United States. *Seism. Res. Lett.* **68**, 333.
- Alexander, S. S. (1985). Relationship among near-field, regional, and teleseismic observations of seismic source parameters, in *The VELA Program*, A. Kerr (Editor), Defense Advanced Projects Agency, 817–829.
- Atkinson, G. M., and R. F. Mereu (1992). The shape of ground motion attenuation curves in Southeastern Canada. *Bull. Seism. Soc. Am.* **82**, 2014–2031.
- Baquer, S., and B. J. Mitchell (1998). Regional variation of  $Lg$  coda  $Q$  in the continental United States and its relation to crustal structure and evolution. *Pure Appl. Geophys.* **153**, 613–638.

- Bennett, T. J., and J. R. Murphy (1986). Analysis of seismic discrimination capabilities using regional data from Western United States events, *Bull. Seism. Soc. Am.* **76**, 1069–1086.
- Boore, D., and G. Atkinson (1992). Source spectra for the 1988 Saguenay, Quebec earthquakes, *Bull. Seism. Soc. Am.* **82**, 683–719.
- Bouchon, M. (1982). The complete synthesis of seismic crustal phases at regional distances, *J. Geophys. Res.* **87**, 1735–1741.
- Campillo, M. (1987). *Lg* wave propagation in laterally varying crust and the distribution of the apparent quality factor in central France, *J. Geophys. Res.* **92**, 12,604–12,614.
- Campillo, M. (1990). Propagation and attenuation characteristics of the crustal phase *Lg*, *Pure Appl. Geophys.* **132**, 1–19.
- Chael, E. (1987). Spectral scaling of earthquakes in the Miramichi region of New Brunswick, *Bull. Seism. Soc. Am.* **77**, 347–365.
- Chavez, D. E., and K. F. Priestley (1986). Measurement of frequency dependent *Lg* attenuation in the Great Basin, *Geophys. Res. Lett.* **13**, 551–554.
- Cong, L., J. Xie, and B. J. Mitchell (1996). Excitation and propagation of *Lg* from earthquakes in central Asia with implication for explosion/earthquakes discrimination, *Geophys. J. Int.* **101**, 27,779–27,789.
- Dreger, D. S., and D. Helmberger (1993). Determination of source parameters at regional distances with three-component sparse network data, *J. Geophys. Res.* **98**, 8107–8125.
- Dwyer, J. J., R. B. Herrmann, and O. W. Nuttli (1983). Spatial attenuation of the *Lg* wave in the Central United States, *Bull. Seism. Soc. Am.* **73**, 781–796.
- Ewing, M., S. W. Jardetzky, and F. Press (1957). *Elastic Waves in Layered Media*, McGraw-Hill, New York, 380.
- Goldberg, D. E. (1989). *Genetic Algorithms in Search, Optimization, and Machine Learning*, Addison-Wesley, Reading, Massachusetts.
- Herrmann, R. B. (1980). *Q* estimates using the coda of local earthquakes, *Bull. Seism. Soc. Am.* **70**, 447–468.
- Herrmann, R. B., and A. Kijko (1983). Modeling some empirical *Lg* relations, *Bull. Seism. Soc. Am.* **56**, 157–171.
- Jin, A., and K. Aki (1988). Spatial and temporal correlation between coda *Q* and seismicity in China, *Bull. Seism. Soc. Am.* **78**, 741–769.
- Kennett, B. L. N. (1986). *Lg* waves and structural boundaries, *Bull. Seism. Soc. Am.* **76**, 1133–1141.
- Knopoff, L. F., F. Schwab, and E. Kausel (1973). Interpretation of *Lg*, *Geophys. J. R. Astron. Soc.* **33**, 389–404.
- Koper, K. D. (1998). Computational aspects of seismology, *Ph.D. Thesis*, Washington University, St. Louis, Missouri.
- Koper, K. D., M. E. Wyssession, and D. A. Wiens (1999). Multimodal function optimization with a niching genetic algorithm: a seismological example, *Bull. Seism. Soc. Am.* **89**, 978–988.
- Mitchell, B. J. (1995). Anelastic structure and evolution of the continental crust and upper mantle from seismic surface wave attenuation, *Rev. Geophys.* **33**, 441–462.
- Mitchell, B. J., J. Xie, S. Baqer (1997). *Lg* excitation, attenuation, and source spectral scaling in central and eastern North America, Report to the Nuclear Regulatory Commission, NUREG/CR-6563, Washington, D.C.
- Mueller, R. A., and J. R. Murphy (1971). Seismic characteristics of underground nuclear explosion. I. Seismic spectrum scaling, *Bull. Seism. Soc. Am.* **61**, 1675–1692.
- Nuttli, O. W. (1973). Seismic wave attenuation and magnitude relations for eastern North America, *J. Geophys. Res.* **78**, 876–885.
- Nuttli, O. W. (1983). Empirical magnitude and spectral scaling relations for mid-plate and plate-margin earthquakes, in *Quantification of Earthquakes*, S. J. Duda and K. Aki (Editors), *Tectonophysics* **93**, 207–223.
- Nuttli, O. W. (1986). Yield estimates of Nevada test site explosions obtained from seismic *Lg* waves, *J. Geophys. Res.* **91**, 2137–2151.
- Nuttli, O. W. (1988). *Lg* magnitudes and yield estimates for underground Novaya Zemlya nuclear explosions, *Bull. Seism. Soc. Am.* **78**, 873–884.
- Ou, G. B., and R. B. Herrmann (1990). A statistical model for ground motion produced by earthquakes at local and regional distances, *Bull. Seism. Soc. Am.* **80**, 1397–1417.
- Patton, H. J., and S. R. Taylor (1995). Analysis of *Lg* spectral ratios from NTS explosions: implication for the source mechanisms of spall and generation of *Lg* waves, *Bull. Seism. Soc. Am.* **85**, 220–236.
- Patton, H. J., and W. R. Walter (1993). Regional moment:magnitude relations for earthquakes and explosions, *Geophys. Res. Lett.* **20**, 277–280.
- Pesceckis, L. L., and P. W. Pomeroy (1984). Determination of *Q* using *Lg* waves and its implications for nuclear yield estimation, *EOS* **65**, 995.
- Press, F., and M. Ewing (1952). Two slow surface waves across north America, *Bull. Seism. Soc. Am.* **42**, 219–228.
- Raoof, M. M., and O. W. Nuttli (1984). Attenuation of high-frequency earthquake waves in South America, *Pure Appl. Geophys.* **122**, 619–644.
- Ritsema, J., and T. Lay (1995). Long-period regional moment tensor inversion for earthquakes in the western United States, *J. Geophys. Res.* **100**, 9853–9864.
- Rogers, A. M., S. C. Harmsen, R. B. Herrmann, and M. E. Meremonte (1987). A study of ground motion attenuation in the southern Great Basin, Nevada-California, using several techniques for estimates of *Q<sub>s</sub>*, log *A<sub>0</sub>*, and coda *Q*, *J. Geophys. Res.* **92**, 3527–3540.
- Savage, J. C. (1972). Relation of corner frequency to fault dimensions, *J. Geophys. Res.* **77**, 3788–3795.
- Sereno, T. J., S. R. Bratt, and T. C. Bache (1988). Simultaneous inversion of regional wave spectra for attenuation and seismic moment in Scandinavia, *J. Geophys. Res.* **93**, 2019–2035.
- Shin, T.-C., and R. B. Herrmann (1987). *Lg* attenuation and source studies using 1982 Miramichi data, *Bull. Seism. Soc. Am.* **77**, 384–397.
- Singh, S. K., and R. B. Herrmann (1983). Regionalization of crustal coda *Q* in the continental United States, *J. Geophys. Res.* **88**, 527–538.
- Stoffa, P. L., and M. K. Sen (1991). Nonlinear multiparameter optimization using genetic algorithms: Inversion of plane-wave seismograms, *Geophysics* **56**, 1794–1810.
- Street, R. L., R. B. Herrmann, and O. W. Nuttli (1975). Spectral characteristics of the *Lg* wave generated by central United States earthquakes, *Geophys. J. R. Astr. Soc.* **41**, 51–63.
- Sykes, L. R., and J. F. Evernden (1982). The verification of a comprehensive nuclear test ban, *Sci. Am.* **247**, 47–55.
- Taylor, S. (1993). Regional data from Lawrence Livermore National Laboratory and Sandia National Laboratory seismic networks, LAUR-93-2150, Los Alamos, New Mexico.
- Taylor, S. T., M. D. Denny, and E. S. Vergino (1986). Regional *m<sub>b</sub>:M<sub>s</sub>* discrimination of NTS explosions and western United States earthquakes: a progress report, Lawrence Livermore National Laboratory.
- Taylor, S. T., N. W. Sherman, and M. D. Denny (1988). Spectral discrimination between NTS explosions and Western United States earthquakes at regional distances, *Bull. Seism. Soc. Am.* **78**, 1563–1579.
- Walter, R. W., K. M. Mayeda, and H. J. Patton (1995). Phase and spectral ratio discrimination between NTS earthquakes and Explosion. I. Empirical observations, *Bull. Seism. Soc. Am.* **85**, 1050–1067.
- Wang, C. Y., and R. B. Herrmann (1988). Synthesis of coda waves in layered medium, *Pure Appl. Geophys.* **128**, 7–42.
- Woods, B. B., and D. V. Helmberger (1997). Regional seismic discriminants using wave-train energy ratios, *Bull. Seism. Soc. Am.* **87**, 589–605.
- Woods, B. B., S. Kedar, and D. V. Helmberger (1993). *M<sub>L</sub>:M<sub>0</sub>* as a regional seismic discriminant, *Bull. Seism. Soc. Am.* **83**, 1167–1183.
- Wyssession, M. E., and K. Koper (1996). Using a genetic algorithm to invert PKP travel times for radial P-wave models of the Earth's core and lowermost mantle, *EOS* **77**, no. 46, (Fall Meeting Suppl.) F677–678.
- Xie, J. (1993). Simultaneous inversion for source spectrum and path *Q* using *Lg* with application to three Semipalatinsk explosions, *Bull. Seism. Soc. Am.* **83**, 1547–1562.
- Xie, J., and O. W. Nuttli (1988). Interpretation of high-frequency coda at

- large distances: stochastic modeling and method of inversion, *Geophys. J. Int.* **95**, 579–595.
- Xie, J., and B. J. Mitchell (1990a). A back-projection method for imaging large-scale lateral variations of *Lg* coda *Q* with application to continental Africa, *Geophys. J. Int.* **100**, 161–181.
- Xie, J., and B. J. Mitchell (1990b). Attenuation of multiphase surface waves in the Basin and Range Province. *Lg* and *Lg* coda, *Geophys. J. Int.* **102**, 121–137.
- Xie, J., L. Cong, and B. J. Mitchell (1996). Spectral characteristics of the excitation and propagation of *Lg* from underground nuclear explosions in central Asia, *J. Geophys. Res.* **101**, 5813–5822.
- Zhao, L., and D. Helmberger (1994). Source estimation from broadband regional seismograms, *Bull. Seism. Soc. Am.* **84**, 91–104.
- Zhao, L., and D. Helmberger (1996). Regional moments, energy levels, and a new discriminant, *Pure Appl. Geophys.* **146**, 281–304.
- Zhang, T., and T. Lay (1995). Why the *Lg* phase does not traverse oceanic crust, *Bull. Seism. Soc. Am.* **85**, 1665–1678.

Department of Earth and Planetary Sciences  
Washington University  
St. Louis, Missouri

Manuscript received 26 April 1999.